Cell

Cortical Dynein and Asymmetric Membrane Elongation Coordinately Position the Spindle in Anaphase

Tomomi Kiyomitsu[1,2,*] and Iain M. Cheeseman[1,2,*]
[1]Whitehead Institute for Biomedical Research, Nine Cambridge Center, Cambridge, MA 02142, USA
[2]Department of Biology, Massachusetts Institute of Technology, Cambridge, MA 02142, USA
*Correspondence: tomomi.kiyomitsu@gmail.com (T.K.), icheese@wi.mit.edu (I.M.C.)
http://dx.doi.org/10.1016/j.cell.2013.06.010

SUMMARY

Mitotic spindle position defines the cell-cleavage site during cytokinesis. However, the mechanisms that control spindle positioning to generate equal-sized daughter cells remain poorly understood. Here, we demonstrate that two mechanisms act coordinately to center the spindle during anaphase in symmetrically dividing human cells. First, the spindle is positioned directly by the microtubule-based motor dynein, which we demonstrate is targeted to the cell cortex by two distinct pathways: a Gαi/LGN/NuMA-dependent pathway and a 4.1G/R and NuMA-dependent, anaphase-specific pathway. Second, we find that asymmetric plasma membrane elongation occurs in response to spindle mispositioning to alter the cellular boundaries relative to the spindle. Asymmetric membrane elongation is promoted by chromosome-derived Ran-GTP signals that locally reduce Anillin at the growing cell cortex. In asymmetrically elongating cells, dynein-dependent spindle anchoring at the stationary cell cortex ensures proper spindle positioning. Our results reveal the anaphase-specific spindle centering systems that achieve equal-sized cell division.

INTRODUCTION

Cell division is a fundamental process that is required to increase cell number and alter cell types. During the development of multicellular organisms, cells undergo both symmetric and asymmetric cell divisions (Horvitz and Herskowitz, 1992; Morin and Bellaïche, 2011). Symmetric cell division generates identical daughter cells for clonal expansion, whereas asymmetric cell division creates distinct daughter cells to increase cell-type diversity. Symmetric and asymmetric cell divisions can vary in the distribution of cell-fate factors (Knoblich, 2008) and the size of the resulting daughter cells, with a subset of asymmetric divisions generating cells of different sizes (Gönczy, 2008; Siller and Doe, 2009). For specification of these different cell-division types, the mitotic spindle must be oriented and positioned within the cell. The spindle position dictates the site at which the cytokinetic cleavage furrow is formed through signals emanating from the spindle midzone and astral microtubules during anaphase (Burgess and Chang, 2005). To achieve a symmetric cell division with two equal-sized daughter cells, the mitotic spindle must be precisely positioned in the center of the dividing cell.

The position of the mitotic spindle is controlled, at least in part, by dynein-dependent cortical pulling forces exerted on astral microtubules (Gönczy, 2008). Dynein consists of a catalytic heavy chain (DHC) and noncatalytic subunits that interact with additional binding partners, such as the dynactin complex, to control the localization and function of the dynein motor (Kardon and Vale, 2009). We and others have previously demonstrated that dynein and dynactin are recruited to the cell cortex by the Gαi-LGN-NuMA complex in symmetrically dividing human cells to generate pulling forces that control spindle position and orientation during metaphase (Kiyomitsu and Cheeseman, 2012; Kotak et al., 2012; Woodard et al., 2010). However, although the loss of LGN randomizes spindle orientation, it does not result in unequal-sized daughter cells (Kiyomitsu and Cheeseman, 2012). This indicates that additional mechanisms must act to center the spindle and generate equivalently sized daughter cells.

Here, we analyzed the mechanisms that position the spindle within the cell during anaphase. We found that two parallel pathways involving LGN and 4.1 family proteins target dynein to the cell cortex to ensure equal-sized cell division. Unexpectedly, we found that cells also control spindle position by asymmetrically elongating their plasma membrane during anaphase to adjust the cellular boundaries and center the spindle within the cell. Thus, to achieve a symmetric cell division, cells coordinately control the movement of the spindle and the position of the cell boundaries to define a central cell-cleavage site.

RESULTS

NuMA and Dynein Are Recruited to the Anaphase Cell Cortex Independently of LGN and Gαi

LGN depletion eliminates dynein heavy chain (DHC)-GFP localization to the cell cortex during metaphase and randomizes spindle orientation (Figure 1A; Kiyomitsu and Cheeseman, 2012). However, most LGN-depleted cells ultimately generate equal-sized daughter cells (Figure 1A; see below), suggesting that

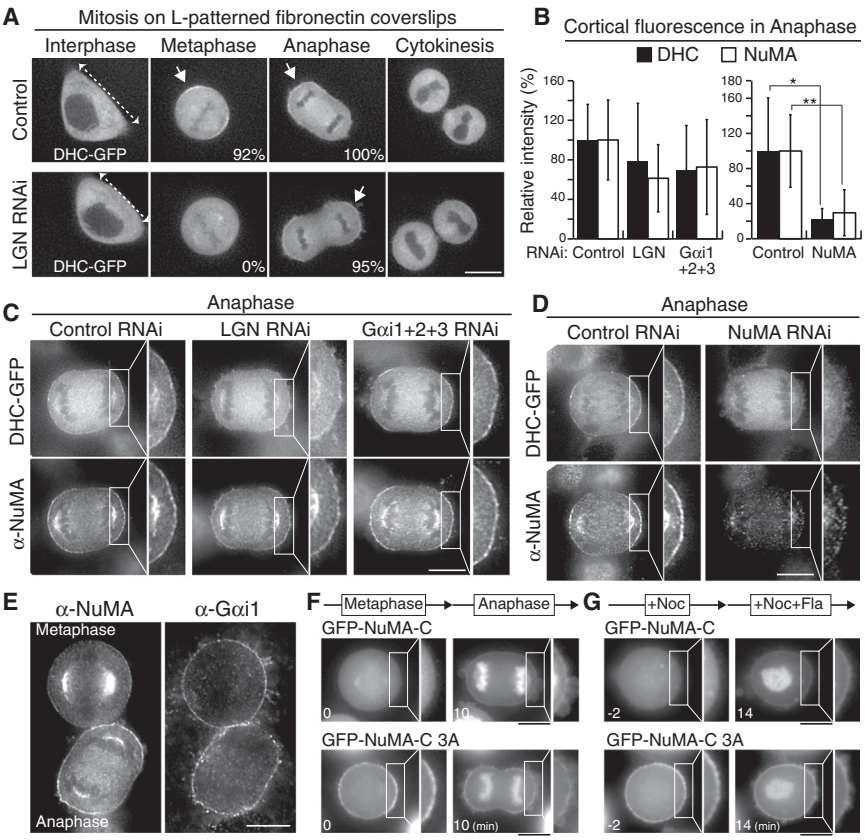

Figure 1. Dynein and NuMA Are Recruited to the Cell Cortex Independently of Gαi and LGN during Anaphase

(A) Fluorescent images of DHC-GFP from time-lapse movies of HeLa cells cultured on L-patterned, fibronectin-coated coverslips. Control cells (upper), but not LGN-depleted cells (lower), divide along the hypotenuse of the L (dashed arrows). Percentages indicate the frequency of cortical dynein localization (indicated by arrows) in controls (n = 25 cells) and LGN-depleted cells (n = 21 cells).

(B) Quantification of DHC-GFP and NuMA cortical fluorescence intensity in the indicated conditions (mean ± SD; n = 12–27 line scans from 4–9 cells); * indicates a statistically significant difference based on a Student's t test (*p = 0.001, **p < 0.0001).

(C and D) Immunofluorescence images of DHC-GFP and NuMA in control HeLa cells and the indicated depletions.

(E) Immunofluorescence images of NuMA and Gαi-1 in metaphase (upper) and anaphase cells (lower).

(F) Fluorescent images of GFP-NuMA-C (upper) and a GFP-NuMA-C 3A mutant (lower) from time-lapse movies.

(G) Time-lapse images of nocodazole (Noc)-arrested cells expressing GFP-NuMA-C (upper) or a GFP-NuMA-C 3A mutant (lower). Nocodazole and flavopiridol (Fla) were added at t = 0 min. Scale bars: 10 μm.

See also Figure S1.

additional mechanisms act to specify the cell-cleavage site in the absence of LGN. Indeed, we found that dynein was recruited to the cell cortex during anaphase in 95% of LGN-depleted cells (Figure 1A). To dissect the requirements for cortical dynein recruitment during anaphase, we analyzed the localization of dynein, dynactin, and NuMA following the depletion of LGN, Gαi, or NuMA by RNAi in HeLa cells. Depletion of LGN or Gαi eliminated the cortical localization of dynein (DHC-GFP), the dynactin subunit p150, and NuMA during metaphase (Figure S1A available online; Kiyomitsu and Cheeseman, 2012), but not anaphase (Figures 1B, 1C, and S1B). In contrast, NuMA depletion reduced the localization of dynein/dynactin to both the metaphase and anaphase cell cortex (Figures 1B, 1D, S1B, and S1C). We note that the residual NuMA that remained following these depletion conditions (Figure 1D) is likely sufficient to suppress the previously defined contribution of NuMA to mitotic spindle assembly (Merdes et al., 1996).

Because we found that NuMA was required for cortical dynein recruitment during anaphase, we next analyzed NuMA localization. NuMA and dynein/dynactin displayed increased levels at the cell cortex during anaphase relative to metaphase (Figures 1E, S1D, and S1E; Collins et al., 2012), whereas Gαi1 and LGN did not (Figures 1E and S1E). This suggests that an additional pool of NuMA and dynein is recruited to the cell cortex at anaphase onset. Consistent with two populations of NuMA, we found that the C-terminal globular region of NuMA (NuMA-C) localized only to the cell cortex during anaphase, but not during metaphase (Figures 1F and S1F–S1H). LGN depletion did not affect the localization of NuMA-C to the anaphase cell cortex (Figure S1I). Inhibition of cyclin-dependent kinase (CDK) activity using flavopiridol (Fla) in cells treated with the microtubule-depolymerizing drug nocodazole caused NuMA-C to accumulate at the cell cortex (Figure 1G), suggesting that this localization is negatively regulated by CDK. The C-terminal region of NuMA contains multiple CDK consensus phosphorylation sites, and a phosphodeficient mutant of full-length NuMA ("3A"; T2015A T2055A S2087A) shows increased accumulation at the cell cortex during metaphase (Compton and Luo, 1995). Consistent with a role for these phosphorylation sites in regulating cortical recruitment, we found that GFP-NuMA-C 3A localized prematurely to the cell cortex during metaphase (Figure 1F, lower). Taken together, these results suggest that the NuMA C-terminal region promotes the LGN-independent targeting of NuMA to the cell cortex during anaphase and is regulated by CDK-dependent phosphorylation.

Band 4.1 Proteins Are Required for the Anaphase-Specific Cortical Localization of NuMA and Dynein

We hypothesized that NuMA-C 3A localizes to the metaphase cell cortex by interacting with cortical receptors that normally bind to dephosphorylated NuMA during anaphase. To identify the cellular binding partners for NuMA-C 3A, we isolated GFP-NuMA-C 3A from HeLa cells arrested in mitosis using nocodazole. Mass spectrometry analysis indicated that GFP-NuMA-C

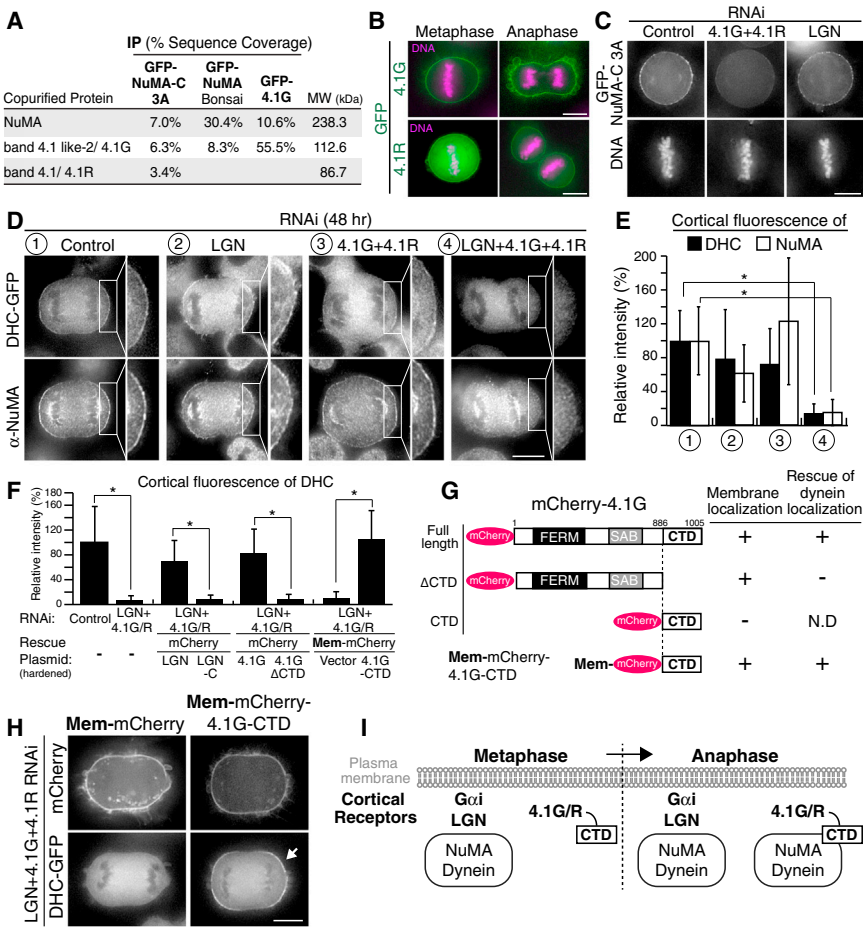

Figure 2. 4.1G and 4.1R Are Anaphase-Specific Cortical Receptors for NuMA and Dynein

(A) Data from mass spectrometry analysis of the indicated affinity purifications listing the percentage sequence coverage.

(B) Fluorescent images of HeLa cells expressing GFP-4.1G (isoform a, NP_001422) or GFP-4.1R (IMAGE clone 40001729).

(C) Fluorescent images of GFP-NuMA-C 3A and DNA in control cells and the indicated RNAi-based depletions.

(D) Immunofluorescence images of DHC-GFP and NuMA in control cells and the indicated depletions.

(E) Quantification of DHC-GFP and NuMA cortical fluorescence intensity in the indicated conditions (mean ± SD; n = 12–36 line scans from 4–12 cells, *$p < 0.0001$).

(F) Quantification of DHC-GFP cortical fluorescence intensity under the indicated conditions (mean ± SD; n = 27–30 line scans from 9–10 cells, *$p < 0.0001$).

(G) Diagram showing full-length 4.1G and the tested truncation fragments. The previously defined FERM ([Four] 4.1 protein, Ezrin, Radixin, Moesin) domain, spectrin-actin binding (SAB) domain, and CTD (Diakowski et al., 2006) are indicated. Right: summary of membrane localization and rescue of cortical dynein localization by the indicated 4.1 fragments.

(H) Fluorescence images showing rescue of DHC-GFP localization by membrane-targeted 4.1G-CTD (arrow) in LGN and 4.1 codepleted cells.

(I) Diagram showing the cortical dynein receptors during metaphase and anaphase. Scale bars: 10 μm.

See also Figure S2.

3A copurified with 4.1G (also known as band 4.1-like 2 protein/ EPB41L2) and 4.1R (also known as band 4.1 protein/ EPB41; Figure 2A), but not with LGN. Similar purifications using an internally truncated version of NuMA lacking a large portion of the coiled-coil (NuMA^{Bonsai}; Figures S1F and S1G) also isolated 4.1G (Figure 2A). GFP-tagged 4.1G and 4.1R localized to the cell cortex throughout mitosis (Figure 2B), similar to the case with endogenous 4.1G (Figure S2A). In reciprocal purifications, we found that GFP-4.1G isolated NuMA, but not LGN (Figure 2A). In our previous GFP-LGN purifications, we isolated NuMA, Gαi, dynein, and dynactin, but not 4.1 proteins (Kiyomitsu and Cheeseman, 2012). Previous two-hybrid studies identified an interaction between NuMA and 4.1 proteins (Mattagajasingh et al., 1999; Ye et al., 1999), but did not test the relationship between these proteins at the cell cortex. Importantly, codepletion of 4.1G and 4.1R, but not LGN depletion, disrupted the cortical localization of GFP-NuMA-C 3A during metaphase (Figures 2C and S2B). These results suggest that band 4.1 proteins associate with the NuMA C terminus to target it to the cell cortex.

Based on the results described above, we hypothesized that there are two parallel pathways for cortical NuMA/dynein/dynactin recruitment in HeLa cells: an LGN-dependent pathway and a 4.1-dependent, anaphase-specific pathway. To test this, we depleted LGN and 4.1 either individually or in combination by RNAi (Figures 2D and S2C). Individual depletion of LGN abolished cortical NuMA and dynein/dynactin localization during metaphase, but not during anaphase (Figures 2D, 2E, and S1A), whereas 4.1G/R depletion did not affect cortical NuMA or dynein/dynactin localization during either metaphase or anaphase (Figure 2D, 2E, S1A, and S2D). In contrast, codepletion of LGN and 4.1G/R abolished the cortical localization of NuMA, dynein, and dynactin during both metaphase and anaphase (Figures 2D, 2E, S1A, and S2D). In LGN and 4.1G/R codepleted cells, expression of RNAi-resistant versions of either mCherry-LGN or mCherry-4.1G restored dynein localization to the cell cortex (Figures 2F, S2E, and S2F). Together, these results suggest that an LGN-dependent pathway targets NuMA and dynein to the cell cortex during metaphase and maintains cortical dynein throughout anaphase, and that a 4.1-dependent pathway recruits a second pool of NuMA and dynein in parallel to the LGN-dependent pathway during anaphase.

Artificial Membrane Targeting of the 4.1G C-Terminal Domain Rescues Cortical Dynein Localization in LGN and 4.1G/R Codepleted Cells

We next sought to define the requirements for the ability of LGN and 4.1 to target NuMA and dynein to the cell cortex. In contrast to replacement with full-length LGN, a LGN-C fragment lacking

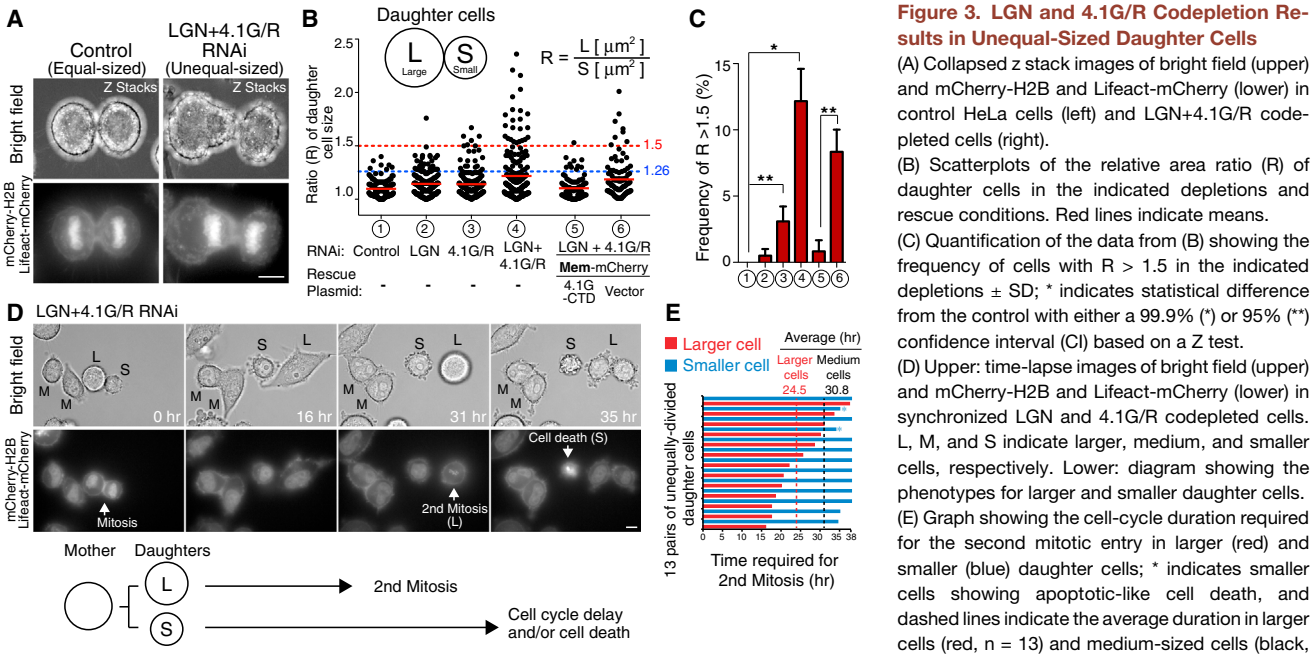

Figure 3. LGN and 4.1G/R Codepletion Results in Unequal-Sized Daughter Cells

(A) Collapsed z stack images of bright field (upper) and mCherry-H2B and Lifeact-mCherry (lower) in control HeLa cells (left) and LGN+4.1G/R codepleted cells (right).

(B) Scatterplots of the relative area ratio (R) of daughter cells in the indicated depletions and rescue conditions. Red lines indicate means.

(C) Quantification of the data from (B) showing the frequency of cells with R > 1.5 in the indicated depletions ± SD; * indicates statistical difference from the control with either a 99.9% (*) or 95% (**) confidence interval (CI) based on a Z test.

(D) Upper: time-lapse images of bright field (upper) and mCherry-H2B and Lifeact-mCherry (lower) in synchronized LGN and 4.1G/R codepleted cells. L, M, and S indicate larger, medium, and smaller cells, respectively. Lower: diagram showing the phenotypes for larger and smaller daughter cells.

(E) Graph showing the cell-cycle duration required for the second mitotic entry in larger (red) and smaller (blue) daughter cells; * indicates smaller cells showing apoptotic-like cell death, and dashed lines indicate the average duration in larger cells (red, n = 13) and medium-sized cells (black, n = 26). Scale bars: 10 μm.

See also Figure S3.

the NuMA-binding N-terminal region localized to the plasma membrane, but failed to restore cortical dynein localization in LGN and 4.1G/R codepleted cells (Figures 2F and S2E). Similarly, expression of mCherry-4.1GΔCTD lacking a ~120 amino acid putative NuMA-binding C-terminal domain (CTD) (Figures 2G and S2G; Mattagajasingh et al., 1999; Ye et al., 1999) localized to the plasma membrane (Figure 2G and S2H), but failed to restore cortical dynein localization in LGN and 4.1G/R codepleted cells (Figures 2F, 2G, and S2F). Although the 4.1G-CTD itself does not localize to the membrane (Figure S2H), artificial targeting of the 4.1G-CTD to the membrane using a membrane-targeting signal (N terminus of neuromodulin; Mem-mCherry-4.1G-CTD) restored cortical dynein and NuMA localization during anaphase in LGN- and 4.1G/R-depleted cells (Figures 2F, 2H, S2I, and S2J). These results indicate that 4.1 proteins recruit NuMA and dynein to the anaphase cell cortex through their conserved CTD (Figure 2I).

LGN and 4.1G/R Codepletion Results in Unequal-Sized Cell Division

Cortical dynein is thought to define daughter-cell size by controlling the spindle position during anaphase (Gönczy, 2008). Up to now, however, it has not been possible to analyze the specific roles of cortical dynein in vertebrate cells, because both dynein and NuMA play multiple roles in spindle structure, organization, and mitotic progression (Merdes et al., 1996). Here, we found that codepletion of LGN and 4.1G/R disrupted the localization of dynein to the cell cortex without affecting spindle structure, providing an ideal tool to test the contribution of cortical dynein to spindle positioning. HeLa cells normally divide to generate daughter cells of equivalent sizes (Figure 3A, left). In contrast, codepletion of LGN and 4.1G/R resulted in unequal-sized daughter cells for a subset of cell divisions (Figure 3A, right). To quantify such unequal-sized cell divisions, we measured the ratio (R) of the areas of the two daughter cells (large [L] and small [S]) in control cells, LGN or 4.1G/R individually depleted cells, or LGN and 4.1G/R codepleted cells (Figure 3B). We found that R had an average value of 1.1 in control cells (Figures 3B and S3A), corresponding to equivalently sized daughter cells. In LGN or 4.1G/R individual depletions, daughter-cell size was subtly affected (Figures 3B, 3C, and S3A). In contrast, LGN and 4.1G/R codepleted cells displayed highly unequal-sized cell divisions, with 11.9% of cell divisions having an R > 1.5, a value that was never observed in control cells (Figures 3A–C and S3A). The amount of DNA in each cell, as visualized by mCherry-histone H2B fluorescence, was similar among these unequal-sized daughters (Figure 3A), indicating that sister chromosome segregation was not affected. Importantly, this unequal-sized cell division in the LGN and 4.1 codepleted cells was rescued by artificial targeting of the 4.1G-CTD to the membrane (Figures 3B, 3C, S3A, and S3B), or by expression of small interfering RNA (siRNA)-resistant full-length 4.1G or LGN, but not 4.1GΔCTD (Figures S3C and S3D). These results suggest that cortical dynein is critical for equal-sized cell division in symmetrically dividing human cells.

To analyze the effects of the unequal-sized cell divisions, we followed the behavior of the "larger" and "smaller" daughter cells in synchronized cultures (Figure 3D). Larger daughter cells (labeled as L) always entered the next mitosis earlier than smaller cells (S, n = 13; average duration = 24.5 hr) and also earlier than normal "medium"-sized daughters (M; average duration = 30.8 hr) resulting from a typical equal-sized cell division (Figure 3E). Larger cell size may reduce the G1 phase for cell growth in HeLa cells and result in earlier entry into the next mitosis, similar to what is observed in yeast (Jorgensen and Tyers,

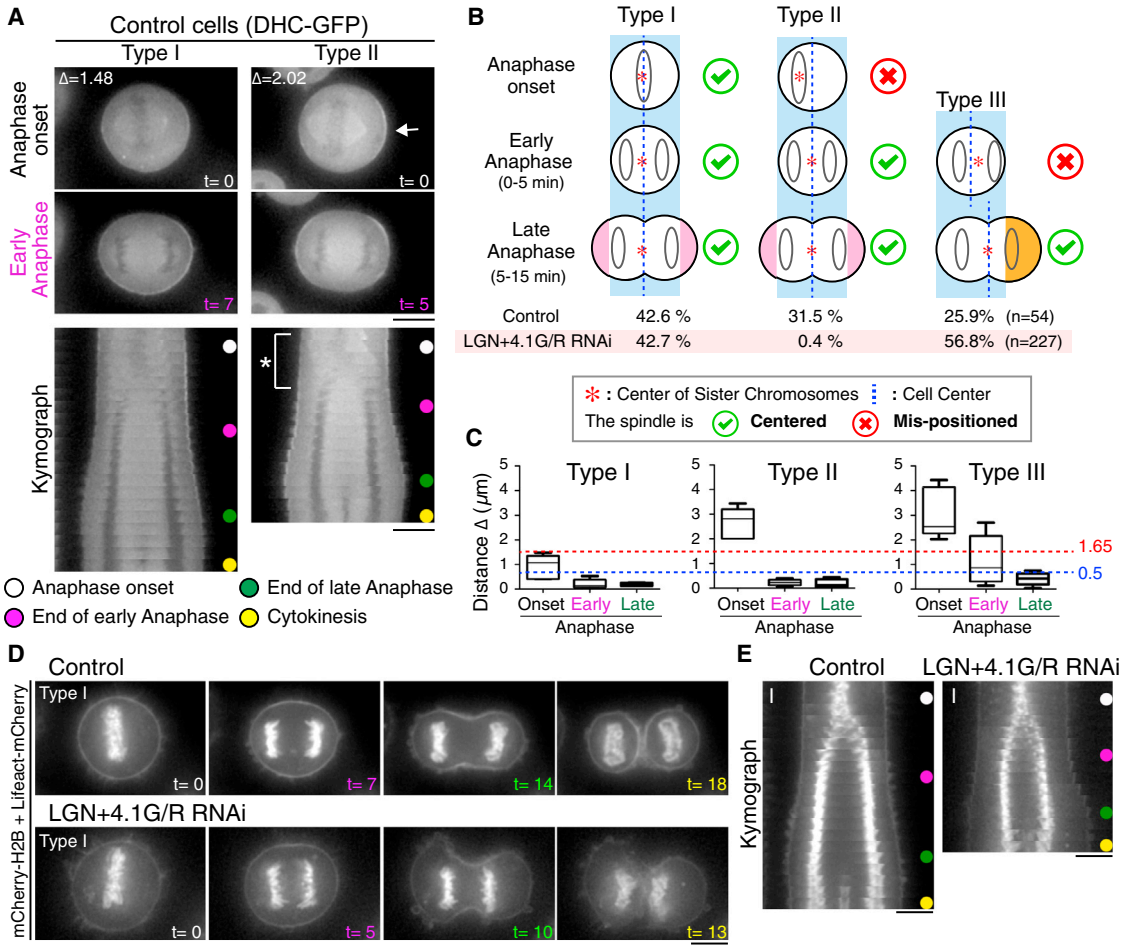

Figure 4. Dynein-Dependent Spindle Movement Drives Spindle Centering during Early Anaphase

(A) Upper: time-lapse images showing DHC-GFP in a type I (left) and type II (right) cell. Lower: kymographs showing the movements of dynein at 1 min intervals. Arrow indicates cortical dynein, * indicates spindle movement during early anaphase.

(B) Diagram summarizing the three types of cell behavior for their anaphase spindle-centering processes. Cells were classified based on the position of chromosomes at anaphase onset and the type of membrane elongation. The frequency of each class in control and LGN and 4.1G/R codepleted cells is indicated.

(C) Box plots of Δ (the distance between the cell center and the center of the sister chromatids) in control cells at anaphase onset, and the end of early and late anaphase. The red and blue dashed lines indicate Δ of 1.65 and 0.5, respectively (see Figure S4A for details). n ≥ 5 cells for each condition.

(D) Time-lapse images of equally dividing type I cells in control (upper; Movie S1) and LGN and 4.1G/R codepleted cells (lower; Movie S2). See also Movie S3.

(E) Kymographs generated from the image sequences in (D) showing chromosome movements and the cell cortex at 1 min intervals. Scale bars: 10 μm.

See also Figure S4.

2004). All smaller-sized cells showed a cell-cycle delay and 15% of the smaller cells underwent an apoptotic-like cell death during the period observed (Figure 3D), suggesting that vertebrate cells may have a minimal cell-size threshold for survival. These results suggest that cortical dynein functions during anaphase to ensure equal-sized cell division, and that the failure to generate proper cell-size symmetry alters cell-cycle progression in daughter cells.

Dynein-Dependent Spindle Movement Drives Spindle Centering during Early Anaphase

To visualize the spindle centering processes, we next monitored dynein (DHC-GFP), chromosomes (mCherry-H2B), and the cell cortex (Lifeact-mCherry; Figures 4A, 4D, and 4E) during anaphase. For this analysis, we classified anaphase into two phases: early anaphase (~0–5 min after anaphase onset, during which time the cell shape does not change), and late anaphase (~5–15 min after anaphase onset, during which time the cells elongate their boundaries; Figure 4B). We found that 42% of control cells (which we term type I) entered anaphase with the spindle centrally positioned (Figures 4A, 4B, and 4D). For these cells, the distance between the cell center and the center of the separating sister chromatid masses (termed Δ; see Figure S4A) was <1.65 μm at anaphase onset (red line in Figure 4C), indicative of a central spindle position. This distance decreased further during early anaphase (blue line in Figure 4C) such that the spindle was precisely centered prior to cell elongation during late anaphase. In contrast, 31% of control cells (which we term

type II) entered anaphase with the spindle mispositioned (Δ > 1.65 μm), but subsequently corrected this positioning during early anaphase (Figures 4B and 4C) by moving the spindle toward the distal cell cortex (Figure 4A, see kymograph). In these cells, dynein localized asymmetrically to the cell cortex at anaphase onset (Figure 4A, right, t = 0, arrow), which, as we previously showed, drives spindle movement during metaphase (Kiyomitsu and Cheeseman, 2012). Thus, the majority of control cells precisely positioned the spindle at the cell center by the end of early anaphase (Figures 4B and 4C). This central spindle position was maintained during late anaphase, during which time the plasma membrane elongated near both spindle poles to increase the cellular boundaries and accommodate spindle elongation (Figures 4D, upper, and 4E, left; Movie S1).

We next sought to assess the role of cortical dynein in spindle centering during early anaphase. In LGN- and 4.1G/R-depleted cells, a subset of cells entered anaphase with a central spindle position (Figures 4B, type I, and 4D, lower). Although these cells lack cortical dynein, the size of the mitotic spindle (~14 μm) relative to the diameter of a HeLa cell (~23 μm) could allow these cells to randomly "center" their spindle. Importantly, in LGN- and 4.1G/R-depleted cells, we almost never observed spindle movements that corrected spindle positioning during early anaphase (Figure 4B, type II). Together, these results show that although 74% of control cells centered their spindle by the end of early anaphase, only 43% of the LGN and 4.1G/R codepleted cells displayed spindle centering at this time point (Figure 4B). Even in cases where the spindle was centrally positioned, we found that sister chromatid separation and spindle elongation were strongly impaired in LGN and 4.1G/R codepleted cells (Figures 4D, 4E, S4C, and S4D; Movies S2 and S3). These results suggest that dynein-based cortical pulling forces contribute to both spindle centering and spindle elongation during anaphase.

Asymmetric Plasma Membrane Elongation Contributes to Spindle Positioning during Late Anaphase

The majority of control cells achieved a central spindle position during early anaphase (Figure 4B). However, 25% of control cells (which we term type III) still had spindle-positioning defects at the end of early anaphase (Figures 4C and S4B). To determine the mechanisms by which this spindle misposition is corrected, we visualized spindle positioning, spindle elongation, and cell-shape reorganization. Unexpectedly, we found that in cells with an off-centered spindle during late anaphase, the plasma membrane elongated asymmetrically such that only one side of the polar membrane region elongated, with the other side remaining stationary (Figure 5A, lower, and 5B, right; Movie S4). This asymmetric membrane elongation is different from the symmetric anaphase membrane elongation that occurs in type I and II cells (Figures 4B, 4D, and 4E), in which both sides of the polar membrane elongate equally during anaphase (Figures 5A, upper, and 5B, left; Movie S5). To our knowledge, such an asymmetric membrane elongation behavior during mitosis in symmetrically dividing cells has not been reported previously. Asymmetric plasma membrane elongation is not the result of cell movement because the cells were stably attached to coverslips throughout mitosis (data not shown). In addition, asymmetric elongation is not due to a heterogeneous extrinsic cellular environment because we also observed this behavior in cells cultured on fibronectin-coated, L-patterned coverslips with similar frequencies (symmetric 56%, asymmetric 44%, n = 25; Figure S5A). We also observed asymmetric membrane elongation during anaphase in nontransformed human Rpe1 cells (Figure S5B).

Although the spindle also elongates concurrently with this asymmetric membrane elongation, the polar membrane elongated faster than the spindle and increased the distance between the growing cell cortex and the nearest set of sister chromatids (Figures 5C, lower kymograph, and S5C). Therefore, asymmetric membrane elongation had the net effect of correcting the spindle position by altering the cellular boundaries relative to the mitotic spindle during anaphase (Figures 4C and 5B). In summary, using a combination of directed spindle movements during early anaphase and asymmetric membrane elongation relative to the spindle during late anaphase, control cells ultimately positioned the spindle centrally, resulting in an equal-sized cell division (Figure 4B).

LGN and 4.1G/R Codepleted Cells Fail to Anchor the Mitotic Spindle in Asymmetrically Elongating Cells

Although LGN- and 4.1G/R-depleted cells showed defective spindle centering during early anaphase, these defects are not sufficient to explain the unequal-sized cell division observed in the depleted cells (Figures 3A, 3B, and 4D). Importantly, we found that >90% of the LGN and 4.1G/R codepleted cells that divided unevenly (R > 1.5) displayed asymmetric membrane elongation (Figures 5D and 5E; Movie S6). This suggests that asymmetric plasma membrane elongation results in unequal-sized cell division in the absence of cortical dynein. In control cells undergoing asymmetric membrane elongation, the distance between the stationary cell cortex and the nearest set of sister chromatids was constant during late anaphase (Figures 5F and 5G, upper). In these asymmetrically elongating cells, dynein localized to the stationary cell cortex (Figure 5H, left, arrows) such that it could act to anchor the spindle and prevent its displacement. Indeed, based on the localization of the microtubule plus-end tracking protein GFP-EB1, it appears that astral microtubules contact the stationary cell cortex during anaphase (Figure S5D). In contrast, we found that in LGN and 4.1G/R codepleted cells (Figure 5H, right), asymmetric membrane elongation resulted in both sets of sister chromatids moving together toward the growing cell cortex (Figure 5G, lower). The distance between the stationary cell cortex and the nearest set of sister chromatids increased during late anaphase in LGN and 4.1G/R codepleted cells (Figure 5F, red). This pairwise movement of sister chromatids resulted in an increased Δ with an average value of 1.97 μm (Figure S4E) and displaced the spindle midzone and cell-cleavage site, resulting in unequal-sized daughter cells (Figure 5D). These results suggest that cortical dynein prevents unequal-sized cell division in asymmetrically elongating cells in part by anchoring the spindle to the stationary cell cortex.

Membrane Blebbing, but Not Exocytosis, Contributes to Asymmetric Cortical Expansion

We next analyzed the mechanisms of asymmetric plasma membrane elongation during anaphase. Expansion of the plasma

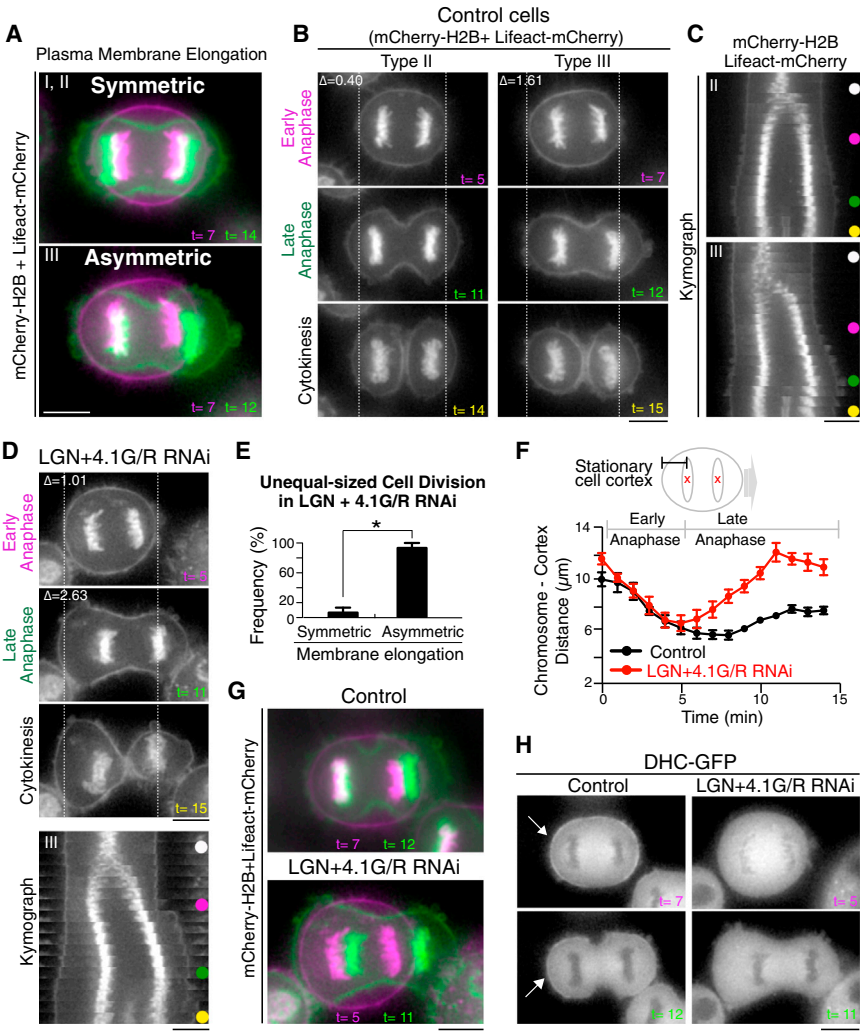

Figure 5. Asymmetric Plasma Membrane Elongation and Cortical Dynein Coordinately Center the Spindle during Late Anaphase

(A) Merged fluorescent images of symmetrically or asymmetrically elongating cells at the end of early anaphase (magenta) and late anaphase (green).

(B) Time-lapse images of type II and type III cells (Movies S4 and S5). Dashed lines indicate cellular boundaries at early anaphase.

(C) Kymographs resulting from image sequences in (B) showing the movements of the chromosomes and the cell cortex at 1 min intervals.

(D) Time-lapse images (upper) and corresponding kymographs (lower; 1 min intervals) showing mCherry-H2B and Lifeact-mCherry in unequally dividing type III cells codepleted for LGN and 4.1G/R (Movie S6). Dashed lines indicate cellular boundaries at early anaphase.

(E) Quantification of membrane elongation in unequally dividing (R > 1.5) cells caused by LGN and 4.1G/R codepletion. Graph shows mean ± SD (n = 16); * indicates statistical difference between symmetric and asymmetric membrane elongation with 99.9% CI based on a Z test.

(F) Graph showing sister chromatid distance from the stationary cell cortex for control (black, n = 5) and unequally dividing LGN and 4.1G/R codepleted cells (red, n = 5). All sequences were time aligned with respect to anaphase onset (t = 0). Error bars represent the SEM.

(G) Merged images of cells at the end of early anaphase (magenta) and late anaphase (green) in asymmetrically elongating control (upper) and LGN and 4.1G/R codepleted cells (lower).

(H) Images showing DHC-GFP in asymmetrically elongating control (left) and LGN and 4.1G/R codepleted cells corresponding to (G). Arrows indicate dynein localization to the stationary cell cortex. Scale bars: 10 μm.

See also Figure S5.

membrane could occur by local secretion of new membrane from internal vesicles or by remodeling of the existing plasma membrane as the cell flattens from its rounded mitotic state. To test whether secretion occurs at sites of polar membrane expansion, we visualized membranes by incubating cells with the membrane dye FM4-64. Internal vesicles were largely excluded from the growing polar cell cortex during asymmetric cell elongation in both HeLa and Rpe1 cells, and instead enriched near the cytokinetic cleavage furrow (Figures S6A–S6C). Therefore, asymmetric membrane elongation involves either remodeling of the pre-existing membrane or newly incorporated membranes deposited near the cleavage furrow, but not direct deposition of new membrane at the site of expansion.

We next analyzed plasma membrane remodeling events. During asymmetric membrane elongation in HeLa cells, we observed the presence of membrane blebs that formed only at the growing polar cell cortex (Figures 6A, 6B, and S6D). Based on the dynamic localization of GFP-Anillin, which provides a marker for retracting blebs (Charras et al., 2006), we found that the membrane blebs were sequentially formed throughout the growing cell cortex with rapid cycles (~60 s) of initiation, expansion, and retraction (Figures 6B and S6E; Movie S7). Bleb formation locally disrupted the cortical localization of LGN and 4.1G at the neck of the blebs, although 4.1G, but not LGN, localized to the bleb membrane (Figures S6F and S6G). Bleb formation disrupted pre-existing cortical actin structures at the neck of the bleb (Figures 6A and S6D; Charras and Paluch, 2008), but subsequently assembled new actin structures at the bleb membrane as visualized by Lifeact-mCherry (Figures 6A [t = 2] and S6D). These cycles of bleb formation and contraction extended the cellular boundary and resulted in cortical expansion (Figures 6A [t = 4], S6D, and S6E), providing one potential mechanism for elongation of the polar membrane. Treatment with low doses of the Rho kinase inhibitor Y27632 at concentrations that inhibit membrane blebbing without affecting cytokinesis (Sedzinski et al., 2011) partially reduced the frequency of asymmetric membrane elongation (Figure S6H), suggesting that bleb formation contributes to asymmetric membrane expansion in HeLa cells. However, Rpe1 cells also undergo asymmetric membrane elongation, but do not display membrane blebbing (Figure S5B),

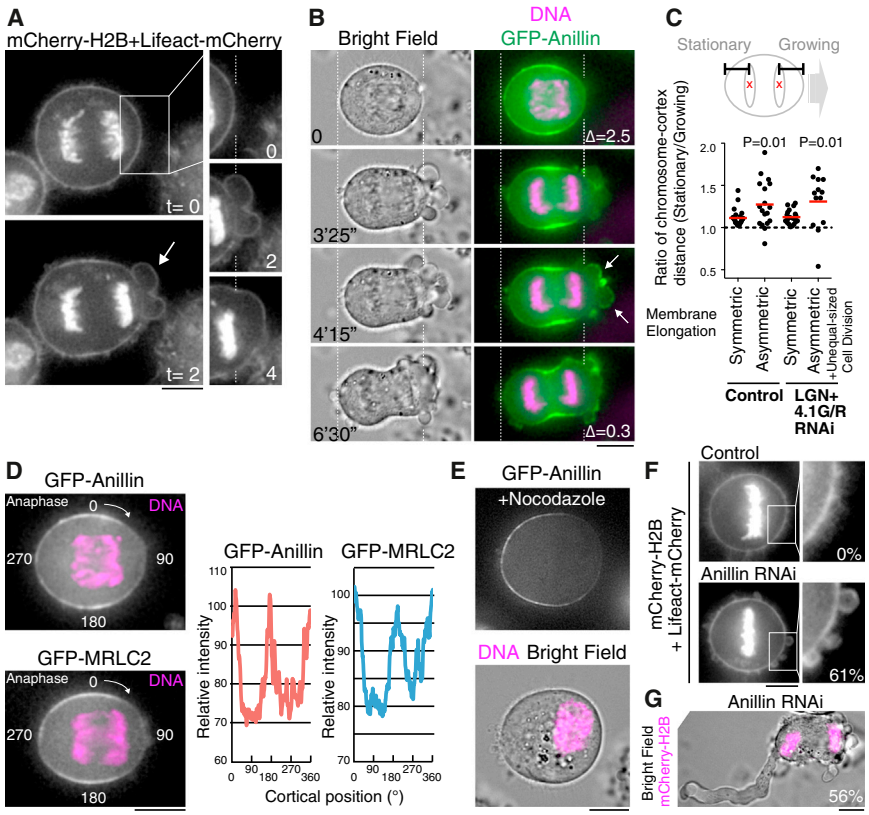

Figure 6. Membrane Blebbing Drives Asymmetric Membrane Elongation

(A) Time-lapse images showing asymmetric membrane blebbing in LGN and 4.1 codepleted cells. Arrow indicates membrane blebs.

(B) Time-lapse images of bright field (left), DNA (magenta), and GFP-Anillin (green) in a control cell. Arrows indicate Anillin localization on retracting membrane blebs (Movie S7).

(C) Scatterplots of the relative ratio of the distance between chromosomes and the stationary or growing cell cortex in symmetrically and asymmetrically elongating control cells (n = 23 and 18, respectively) and LGN and 4.1 codepleted cells (n = 20 and 13, respectively). Red lines indicate means; p values indicate statistical significance based on a Student's t test.

(D) Images of an anaphase cell just prior to asymmetric membrane elongation showing DNA (magenta) and GFP-Anillin (upper) or GFP-MRLC2 (lower). Right: line scan showing the relative fluorescence intensity of cortical GFP-Anillin and GFP-MRLC2 around the cell cortex.

(E) Images of a nocodazole-arrested cell showing GFP-Anillin (upper), and bright field and DNA (magenta; lower).

(F) Images of mCherry-H2B and Lifeact-mCherry showing membrane blebbing at metaphase in control (upper, n = 20) and Anillin-depleted (lower, n = 20) cells. Percentages indicate the frequency of blebbing cells in each condition.

(G) Images showing the formation of large membrane blebs in Anillin-depleted anaphase cells (56%, n = 16). Scale bars: 10 μm.

See also Figure S6.

suggesting that additional mechanisms to promote membrane expansion also exist.

Chromosome-Derived Ran-GTP Signals Reduce Anillin Localization to the Cell Cortex and Induce Asymmetric Membrane Elongation

To define the basis for the asymmetric membrane elongation, we next analyzed the distance between the sister chromatids and the growing or stationary cell cortex at the start of membrane elongation (Figure 6C). We found that increased proximity of chromosomes to the cell cortex strongly correlated with the asymmetric membrane elongation of the nearest cell cortex in control and LGN and 4.1G/R codepleted cells (Figures 6A–6C). This suggests that plasma membrane remodeling is sensitive to the proximity of the chromosomes on the spindle.

We hypothesized that the proximity of the chromosomes to the cell cortex may locally alter proteins that control cortical stiffness and contractility at the polar cell cortex, resulting in membrane blebbing and other remodeling events. To test this, we analyzed the cortical proteins Anillin and myosin (D'Avino, 2009; Salbreux et al., 2012). In symmetrically elongating anaphase cells, GFP-Anillin and GFP-myosin regulatory light chain 2 (MRLC2) show reduced cortical localization to both polar regions (Figure S6I). However, GFP-Anillin and GFP-MRLC2 were asymmetrically reduced at the growing cell cortex just prior to asymmetric membrane elongation (Figures 6D and S6J), and appeared to depend upon the relative proximity of the mitotic spindle to the cell cortex. To test whether the local cortical reduction of these proteins is influenced by signals from the spindle poles, astral microtubules, or chromosomes, we treated cells with nocodazole to depolymerize the microtubules. GFP-Anillin was locally reduced from the cell cortex in the vicinity of chromosome masses in nocodazole-treated HeLa cells (Figure 6E) and Rpe1 cells (Figure S6K). GFP-MRLC2 was also reduced in the vicinity of chromosome masses, and this behavior was enhanced following CDK inhibition in both HeLa and Rpe1 cells (Figure S6L). This local reduction of Anillin and myosin has the potential to contribute to membrane remodeling events, including membrane blebbing. Indeed, we found that in addition to its established role in cytokinesis (Piekny and Glotzer, 2008), global Anillin depletion resulted in premature bleb formation during metaphase (Figure 6F), which was never observed in control cells, and the formation of large membrane blebs during anaphase (Figure 6G).

Previous work has shown that Ran regulates Anillin-mediated pseudocleavage formation in *Drosophila* syncytial embryos (Silverman-Gavrila et al., 2008). To analyze the contribution of chromosome-derived Ran-GTP signals in mammalian cells, we used tsBN2 cells, which contain a temperature-sensitive mutation in RCC1 that prevents the formation of Ran-GTP at the restrictive temperature (Nishitani et al., 1991). In nocodazole-treated tsBN2 cells, Anillin was reduced from the cell cortex in

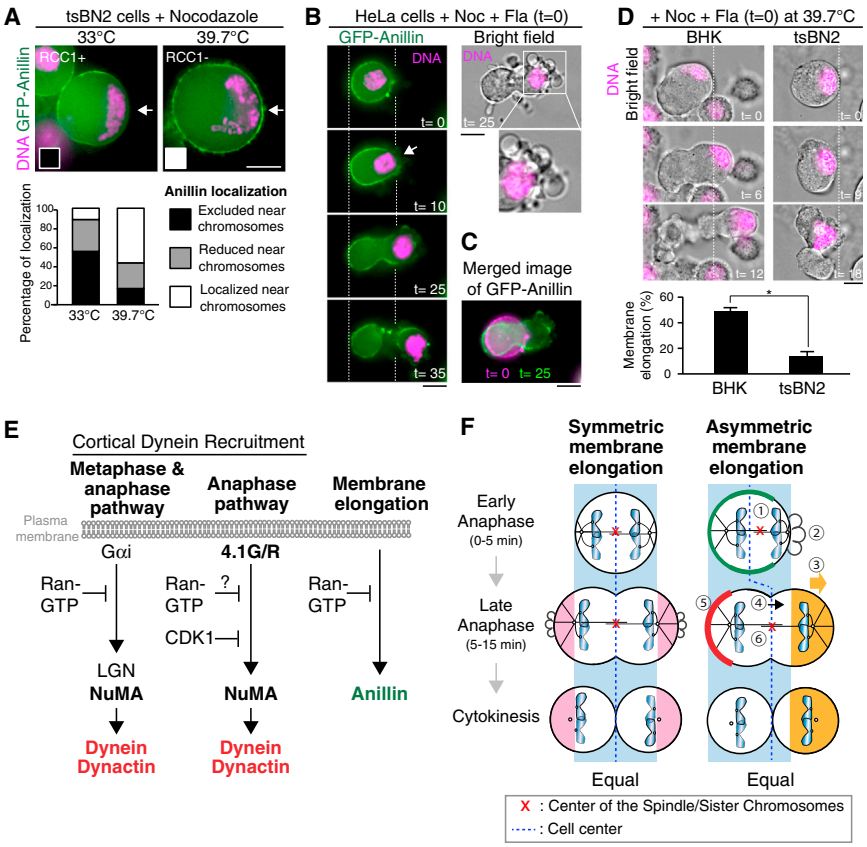

Figure 7. Chromosome-Derived Ran-GTP Signals Locally Reduce Cortical Anillin to Drive Membrane Elongation

(A) Upper: fluorescence images of tsBN2 (RCC1^{ts}) cells stably expressing GFP-Anillin. Cells were arrested with nocodazole and then either maintained at the permissive temperature (33°C; n = 51) or shifted to the restrictive temperature (39.7°C; n = 56). Cells with their chromosomes mass near the cell cortex were observed (arrows). Lower: histogram showing the quantification of the localization data.

(B) Time-lapse images of GFP-Anillin (green), DNA (magenta), and bright field in nocodazole- and flavopiridol-treated cells (Movie S8). Cortical GFP-Anillin is locally reduced in the vicinity of the chromosomes (arrow).

(C) Merged images from (B) at t = 0 (magenta) and t = 25 min (green).

(D) Upper: time-lapse images of nocodazole-and flavopiridol-treated BHK (left) and tsBN2 cells at 39.7°C. Dashed lines indicate boundary of cells at t = 0. Lower: graphs show the frequency of the cells with membrane elongation near the chromosome mass. Graph shows mean ± SD (n > 54); * indicates statistical difference between BHK and tsBN2 cells with 99.9% CI based on a Z test.

(E) Diagram showing pathways for cortical dynein recruitment and membrane elongation.

(F) Model showing anaphase spindle centering mechanisms. Left: when spindle centering occurs during early anaphase via dynein-dependent forces, cells symmetrically elongate the polar membrane. Right: when the spindle is mispositioned at the end of early anaphase, the proximity of the chromosomes to the cell cortex (1) induces asymmetric Anillin localization (green) (2) to expand the cellular boundary (3). Although cortical expansion centers the spindle, it also causes cytosolic flow (4) toward the growing cell cortex. Dynein (red) localizes to the stationary cell cortex to anchor the spindle (5) and prevent displacement. These coordinated actions lead to spindle elongation (6) and spindle centering during late anaphase.

Scale bars, 10 μm. See also Figure S7.

the vicinity of the chromosome masses at the permissive temperature (Figure 7A, left), similar to what was observed for HeLa cells (Figure 6E). However, at the restrictive temperature, Anillin localized to the cell cortex even in the vicinity of chromosomes (Figure 7A, right). The temperature shift did not affect cortical Anillin localization in the parental BHK cells, which are wild-type for RCC1 (data not shown). In contrast to disrupting Ran-GTP, treatment with inhibitors against Aurora B kinase, which forms a spatial gradient on metaphase chromosomes and the anaphase midzone (Fuller et al., 2008), did not strongly affect asymmetric Anillin localization (Figure S7A). These results suggest that chromosome-derived Ran-GTP signals act to locally reduce Anillin from the cell cortex near chromosomes.

To test whether the proximity of chromosomes to the cell cortex is sufficient to cause asymmetric membrane elongation in the absence of the mitotic spindle during anaphase, we treated cells with nocodazole and induced mitotic exit by addition of the CDK inhibitor flavopiridol. In cases in which the chromosome mass was located at the center of the cell, membrane blebs and changes in plasma membrane organization were observed throughout the cell cortex (Figure S7B; Niiya et al., 2005). In contrast, when the chromosome mass was located near the cell cortex, the plasma membrane underwent a dramatic asymmetric expansion in the vicinity of the chromosomes (Figures 7B, 7C, S7B, and S7C; Movie S8) in the regions where Anillin, MRLC2, LGN, and dynein were locally excluded (Figures 7B, S6L, S7C, and S7D). As the chromosome-proximal cell cortex expanded, adjacent regions of the cell cortex contracted, resulting in a "budding" event reminiscent of cytokinesis (Figures 7B [t = 35], S7C, and S7D). Although these asymmetric budding events result from artificial drug treatment, this process is similar to the membrane reorganization events that normally occur during anaphase and cytokinesis (Petronczki et al., 2008), as it requires Plk1, Ect2, and Myosin II activity (Figures S7E–S7G). We observed this asymmetric membrane elongation in both HeLa cells (Figures 7B, S7C, and S7D) and Rpe1 cells (Figure S7H). This asymmetric membrane expansion correlated with the formation of membrane blebs in HeLa cells (Figures 7B and S7C) but not in Rpe1 cells (Figure S7H), similar to the case with unperturbed cells.

To test the contribution of Ran-GTP signals to this asymmetric membrane elongation, we analyzed membrane elongation in BHK and tsBN2 cells following nocodazole and flavopiridol treatment. In BHK cells, the plasma membrane elongated in the vicinity of the chromosome mass (Figure 7D). However, in tsBN2 cells at the restrictive temperature, the membrane did

not elongate regardless of the proximity of the chromosome mass to the cell cortex (Figure 7D). Taken together, these results suggest that when the spindle is displaced, chromosome-derived Ran-GTP signals locally reduce Anillin and other proteins from the polar cell cortex, which results in asymmetric membrane elongation to alter the cellular boundaries and correct spindle positioning during anaphase (Figure 7F).

DISCUSSION

4.1G and 4.1R Are Anaphase-Specific Cortical Receptors for NuMA and Dynein

Here, we identified 4.1G and 4.1R as anaphase-specific cortical receptors for NuMA (Figure 2A), which in turn recruits dynein/dynactin to the cell cortex (Figure 2D). Our data suggest that CDK-dependent phosphorylation of the C-terminal region of NuMA at metaphase prevents NuMA from interacting with 4.1G/R (Figures 1F and 1G) such that the 4.1G/R-NuMA pathway recruits dynein only during anaphase. 4.1 is a well-conserved multifunctional membrane protein (Diakowski et al., 2006), and 4.1R links the plasma membrane to spectrin-actin cytoskeleton in red blood cells (Bennett and Baines, 2001). We demonstrated that the highly conserved 4.1 CTD (Figure S2G) is necessary and sufficient to recruit NuMA and dynein to the anaphase cell cortex (Figures 2F–2H, S2I, and Figure S2J). Although 4.1 and LGN display independent localization (Figures S2E and S2F), suggesting that these two dynein recruitment pathways are functionally distinct, they may act synergistically to recruit cortical dynein during anaphase, based on the observed defects in dynein localization when these pathways are depleted.

Both the LGN- and 4.1-dependent pathways for cortical dynein recruitment utilize NuMA as an adaptor molecule (Figure 7E). Thus, cells could regulate both pathways simultaneously by controlling NuMA, such as through chromosome-derived Ran-GTP signals (Kiyomitsu and Cheeseman, 2012). In contrast, the presence of these dual pathways could allow cells to temporally and spatially control cortical pulling forces. For example, the 4.1-NuMA interaction, but not LGN-NuMA binding, is negatively regulated by CDK during metaphase, which may increase cortical pulling forces during anaphase to ensure proper spindle elongation. In addition, 4.1 proteins, but not LGN, localize to membrane blebs (Figure S6F), which may facilitate rapid dynein recruitment to the newly formed cell cortex. There may also be additional temporal and spatial signals that act to control these different dynein recruitment pathways. For example, signals derived from central spindle may negatively regulate the interaction between NuMA and 4.1 at the equatorial cell cortex during anaphase (Figures 2B, 2D, and 2H). Differential regulation of these two pathways could also be used to generate asymmetric cortical pulling forces during development. We hypothesize that these LGN- and 4.1-dependent cortical dynein recruitment pathways play important roles in tissues and multicellular organisms for both symmetric and asymmetric cell divisions. LGN, 4.1G, and 4.1R individual knockout mice are viable (Konno et al., 2008; Shi et al., 1999; Yang et al., 2011), although LGN knockout mice display randomized spindle orientation for the normally planar neuroepithelial divisions (Konno et al., 2008). In the future, it will be important to test the combined defects caused by simultaneously disrupting LGN and 4.1 proteins during development and in an intact organism.

Asymmetric Plasma Membrane Elongation Acts for Spindle Centering

In addition to dynein-dependent spindle movements, we found that spindle mispositioning that persists into late anaphase can be corrected by asymmetric elongation of the polar plasma membrane. This asymmetric membrane elongation does not appear to be a result of the extrinsic cellular environment (Figure S5A), but instead results from the mispositioning of the anaphase spindle and separation of sister chromatids within the cell (Figure 6C). This asymmetric cortical expansion likely can occur via several mechanisms, but does not appear to involve vesicle secretion at the polar cell membrane (Figures S6A–S6C), and instead requires remodeling of the existing cell membrane. In some cell types, we found that membrane blebbing contributes to asymmetric membrane elongation in response to an off-centered position of the spindle and sister chromatids (Figures 6A, 6B, and S6H). Membrane blebbing at the polar cell cortex during cytokinesis has been proposed to stabilize cell shape by acting as a "release valve" for cortical contractility (Sedzinski et al., 2011). Our results reveal an additional function for membrane blebbing during cytokinesis to control spindle positioning: sequential membrane blebbing disrupts the pre-existing actin cell cortex and forms a new cell cortex to expand the cellular boundary (Figures 6A, 6B, S6D, and S6E). However, even in the absence of membrane blebbing, asymmetric expansion of the plasma membrane can occur through membrane remodeling (Figures 7D, S5B, and S7H).

We propose that during anaphase, a local reduction of cortical Anillin downstream of chromosome-derived Ran-GTP signals locally weakens the polar cell cortex and results in membrane expansion. In previous work, Kaláb et al. (2006) tested the existence of a chromosome-derived Ran-GTP gradient during metaphase. A gradient of RanGTP also persists into early anaphase, based on results obtained with established FRET sensors in HeLa cells (P. Kalab, personal communication). However, additional signals from the spindle pole or astral microtubules may also affect the localization or activity of Anillin and other cortical proteins for cortical expansion. Anillin interacts with activated form of myosin to promote cortical contraction during cytokinesis (Straight et al., 2005). We propose that asymmetric localization of Anillin downstream of Ran-GTP also generates cortical myosin asymmetry during anaphase (Figures 6D, S6J, and S6L), which drives cortical contraction and relaxation at the stationary and growing cell cortex, respectively, for asymmetric membrane elongation (Figure S6M). Importantly, in addition to the work shown here in equally dividing human cells, asymmetric cortical extension also occurs to generate unequal-sized daughter cells during asymmetric cell division in *Caenorhabditis elegans* and *Drosophila* neuroblasts (Connell et al., 2011; Ou et al., 2010; Kotadia et al., 2012). How cortical pulling forces and membrane elongation are differently regulated in symmetric and asymmetric cell divisions will be an exciting topic for future work. Finally, anaphase spindle elongation may also be critical for equal-sized cell division (Figure 4D; Xiao et al., 2012) to generate a larger spindle structure that is more naturally placed in the middle of the dividing cell.

In conclusion, our results reveal that cortical dynein and membrane elongation coordinately control spindle positioning. Both mechanisms are autonomously regulated in response to spindle position and cooperatively center the spindle to achieve an equal-sized cell division.

EXPERIMENTAL PROCEDURES

Cell Culture and siRNA Transfection

HeLa, Rpe1, BHK, and tsBN2 cells were maintained as described previously (Kiyomitsu and Cheeseman, 2012). Clonal cell lines stably expressing GFP^{LAP} or mCherry fusions were generated as described previously (Schmidt et al., 2010). Plasmid DNA transfections were conducted using Effectene (QIAGEN). To inactivate RCC1, tsBN2 cells were cultured at 39.7°C for 2–3.5 hr. To induce mitotic exit in the absence of microtubules, HeLa or Rpe1 cells were incubated for 3–6 hr with 100 nM nocodazole (Sigma Aldrich) and subsequently treated with 100 nM nocodazole plus 5 μM flavopiridol (Sigma Aldrich). Where indicated, cells were incubated with 16 μM FM4-64 (Molecular Probes), 10 μM Y27632 (EMD Biosciences), 10 μM BI2536 (Tocris), or 100 μM blebbistatin (Sigma Aldrich).

RNAi experiments were conducted using the RNAi MAX transfection reagent (Invitrogen) in asynchronous cultures or combined with a double thymidine block to deplete proteins in synchronized cultures. For rescue experiments, plasmids were transfected 1 hr prior to siRNA transfection. For information regarding the siRNAs used, see the Extended Experimental Procedures.

Immunofluorescence and Microscopy

For live-cell imaging, cells were cultured in CO_2-independent media (Invitrogen) with 50–100 ng/ml Hoechst33342 for 30 min prior to observation. Cells were fixed with 3% paraformaldehyde with 2% sucrose. Where indicated, cells were plated on L-patterned, fibronectin-coated coverslips (CYTOO). For information regarding the antibodies used, see the Extended Experimental Procedures.

Images were acquired on a DeltaVision Core microscope (Applied Precision) equipped with a CoolSnap HQ2 CCD camera. For fixed cells, 30 Z sections were acquired in 0.5 μm steps using an Olympus 40×, 1.35 NA U-PlanApo objective. For live-cell imaging, one to three Z sections were acquired in 1–2 μm steps at 1–5 min intervals. For Figure 6B, a single focal image was obtained at 5 s intervals. For the long-term time-lapse imaging in Figure 3D, images were acquired at 30 min intervals for 38 hr. Images were deconvolved using DeltaVision software. Equivalent exposure conditions and scaling were used as appropriate. Distance measurements were analyzed using Softworx (Applied Precision) and ImageJ/Fiji software. To measure the area ratio of daughter cells, Z sections of bright-field images were acquired in 1 μm steps to capture the entire cells during cytokinesis in living cells. Projected images were generated using Softworx (Applied Precision) and cell area was measured with ImageJ/Fiji software. Line scans for cortical fluorescence intensity and kymographs were generated using Metamorph (Molecular Devices) and Photoshop (Adobe), respectively. Movie files were generated using Softworx (Applied Precision) and GraphicConverter.

Affinity Purifications and Mass Spectrometry

GFP^{LAP}-tagged NuMA-C 3A, $NuMA^{Bonsai}$, and 4.1G were isolated from HeLa cells as described previously (Kiyomitsu and Cheeseman, 2012). Purified proteins were identified by mass spectrometry on an LTQ XL ion trap mass spectrometer (Thermo) using MudPIT and SEQUEST software.

Statistics

To determine the significance between the data obtained for two experimental conditions, a Student's t test (GraphPad Software) or Z test (McCallum Layton) was used as indicated in the figure legends.

SUPPLEMENTAL INFORMATION

Supplemental Information includes Extended Experimental Procedures, seven figures, and eight movies and can be found with this article online at http://dx.doi.org/10.1016/j.cell.2013.06.010.

ACKNOWLEDGMENTS

We thank Defne Yarar, Adam Martin, Jonathan Coravos, and members of the Cheeseman laboratory for discussions and critical readings of the manuscript. We also thank Duane Compton for providing reagents. This work was supported by a Scholar award to I.M.C. from the Leukemia & Lymphoma Society, an award from the Human Frontiers Science Foundation, a grant from the NIH/National Institute of General Medical Sciences (GM088313), and a Research Scholar Grant (121776) from the American Cancer Society. I.M.C. is a Thomas D. and Virginia W. Cabot Career Development Professor of Biology. T.K. is supported by a long-term fellowship from the Human Frontiers Science Program.

Received: February 2, 2013
Revised: April 28, 2013
Accepted: June 10, 2013
Published: July 18, 2013

REFERENCES

Bennett, V., and Baines, A.J. (2001). Spectrin and ankyrin-based pathways: metazoan inventions for integrating cells into tissues. Physiol. Rev. *81*, 1353–1392.

Burgess, D.R., and Chang, F. (2005). Site selection for the cleavage furrow at cytokinesis. Trends Cell Biol. *15*, 156–162.

Charras, G., and Paluch, E. (2008). Blebs lead the way: how to migrate without lamellipodia. Nat. Rev. Mol. Cell Biol. *9*, 730–736.

Charras, G.T., Hu, C.K., Coughlin, M., and Mitchison, T.J. (2006). Reassembly of contractile actin cortex in cell blebs. J. Cell Biol. *175*, 477–490.

Collins, E.S., Balchand, S.K., Faraci, J.L., Wadsworth, P., and Lee, W.L. (2012). Cell cycle-regulated cortical dynein/dynactin promotes symmetric cell division by differential pole motion in anaphase. Mol. Biol. Cell *23*, 3380–3390.

Compton, D.A., and Luo, C. (1995). Mutation of the predicted p34cdc2 phosphorylation sites in NuMA impair the assembly of the mitotic spindle and block mitosis. J. Cell Sci. *108*, 621–633.

Connell, M., Cabernard, C., Ricketson, D., Doe, C.Q., and Prehoda, K.E. (2011). Asymmetric cortical extension shifts cleavage furrow position in Drosophila neuroblasts. Mol. Biol. Cell *22*, 4220–4226.

D'Avino, P.P. (2009). How to scaffold the contractile ring for a safe cytokinesis—lessons from Anillin-related proteins. J. Cell Sci. *122*, 1071–1079.

Diakowski, W., Grzybek, M., and Sikorski, A.F. (2006). Protein 4.1, a component of the erythrocyte membrane skeleton and its related homologue proteins forming the protein 4.1/FERM superfamily. Folia Histochem. Cytobiol. *44*, 231–248.

Fuller, B.G., Lampson, M.A., Foley, E.A., Rosasco-Nitcher, S., Le, K.V., Tobelmann, P., Brautigan, D.L., Stukenberg, P.T., and Kapoor, T.M. (2008). Midzone activation of aurora B in anaphase produces an intracellular phosphorylation gradient. Nature *453*, 1132–1136.

Gönczy, P. (2008). Mechanisms of asymmetric cell division: flies and worms pave the way. Nat. Rev. Mol. Cell Biol. *9*, 355–366.

Horvitz, H.R., and Herskowitz, I. (1992). Mechanisms of asymmetric cell division: two Bs or not two Bs, that is the question. Cell *68*, 237–255.

Jorgensen, P., and Tyers, M. (2004). How cells coordinate growth and division. Curr. Biol. *14*, R1014–R1027.

Kaláb, P., Pralle, A., Isacoff, E.Y., Heald, R., and Weis, K. (2006). Analysis of a RanGTP-regulated gradient in mitotic somatic cells. Nature *440*, 697–701.

Kardon, J.R., and Vale, R.D. (2009). Regulators of the cytoplasmic dynein motor. Nat. Rev. Mol. Cell Biol. *10*, 854–865.

Kiyomitsu, T., and Cheeseman, I.M. (2012). Chromosome- and spindle-pole-derived signals generate an intrinsic code for spindle position and orientation. Nat. Cell Biol. *14*, 311–317.

Knoblich, J.A. (2008). Mechanisms of asymmetric stem cell division. Cell *132*, 583–597.

Konno, D., Shioi, G., Shitamukai, A., Mori, A., Kiyonari, H., Miyata, T., and Matsuzaki, F. (2008). Neuroepithelial progenitors undergo LGN-dependent planar divisions to maintain self-renewability during mammalian neurogenesis. Nat. Cell Biol. *10*, 93–101.

Kotadia, S., Montembault, E., Sullivan, W., and Royou, A. (2012). Cell elongation is an adaptive response for clearing long chromatid arms from the cleavage plane. J Cell. Biol. *199*, 745–753.

Kotak, S., Busso, C., and Gönczy, P. (2012). Cortical dynein is critical for proper spindle positioning in human cells. J. Cell Biol. *199*, 97–110.

Mattagajasingh, S.N., Huang, S.C., Hartenstein, J.S., Snyder, M., Marchesi, V.T., and Benz, E.J. (1999). A nonerythroid isoform of protein 4.1R interacts with the nuclear mitotic apparatus (NuMA) protein. J. Cell Biol. *145*, 29–43.

Merdes, A., Ramyar, K., Vechio, J.D., and Cleveland, D.W. (1996). A complex of NuMA and cytoplasmic dynein is essential for mitotic spindle assembly. Cell *87*, 447–458.

Morin, X., and Bellaïche, Y. (2011). Mitotic spindle orientation in asymmetric and symmetric cell divisions during animal development. Dev. Cell *21*, 102–119.

Niiya, F., Xie, X., Lee, K.S., Inoue, H., and Miki, T. (2005). Inhibition of cyclin-dependent kinase 1 induces cytokinesis without chromosome segregation in an ECT2 and MgcRacGAP-dependent manner. J. Biol. Chem. *280*, 36502–36509.

Nishitani, H., Ohtsubo, M., Yamashita, K., Iida, H., Pines, J., Yasudo, H., Shibata, Y., Hunter, T., and Nishimoto, T. (1991). Loss of RCC1, a nuclear DNA-binding protein, uncouples the completion of DNA replication from the activation of cdc2 protein kinase and mitosis. EMBO J. *10*, 1555–1564.

Ou, G., Stuurman, N., D'Ambrosio, M., and Vale, R.D. (2010). Polarized myosin produces unequal-size daughters during asymmetric cell division. Science *330*, 677–680.

Petronczki, M., Lénárt, P., and Peters, J.M. (2008). Polo on the rise—from mitotic entry to cytokinesis with Plk1. Dev. Cell *14*, 646–659.

Piekny, A.J., and Glotzer, M. (2008). Anillin is a scaffold protein that links RhoA, actin, and myosin during cytokinesis. Curr. Biol. *18*, 30–36.

Salbreux, G., Charras, G., and Paluch, E. (2012). Actin cortex mechanics and cellular morphogenesis. Trends Cell Biol. *22*, 536–545.

Schmidt, J.C., Kiyomitsu, T., Hori, T., Backer, C.B., Fukagawa, T., and Cheeseman, I.M. (2010). Aurora B kinase controls the targeting of the Astrin-SKAP complex to bioriented kinetochores. J. Cell Biol. *191*, 269–280.

Sedzinski, J., Biro, M., Oswald, A., Tinevez, J.Y., Salbreux, G., and Paluch, E. (2011). Polar actomyosin contractility destabilizes the position of the cytokinetic furrow. Nature *476*, 462–466.

Shi, Z.T., Afzal, V., Coller, B., Patel, D., Chasis, J.A., Parra, M., Lee, G., Paszty, C., Stevens, M., Walensky, L., et al. (1999). Protein 4.1R-deficient mice are viable but have erythroid membrane skeleton abnormalities. J. Clin. Invest. *103*, 331–340.

Siller, K.H., and Doe, C.Q. (2009). Spindle orientation during asymmetric cell division. Nat. Cell Biol. *11*, 365–374.

Silverman-Gavrila, R.V., Hales, K.G., and Wilde, A. (2008). Anillin-mediated targeting of peanut to pseudocleavage furrows is regulated by the GTPase Ran. Mol. Biol. Cell *19*, 3735–3744.

Straight, A.F., Field, C.M., and Mitchison, T.J. (2005). Anillin binds nonmuscle myosin II and regulates the contractile ring. Mol. Biol. Cell *16*, 193–201.

Woodard, G.E., Huang, N.N., Cho, H., Miki, T., Tall, G.G., and Kehrl, J.H. (2010). Ric-8A and Gi alpha recruit LGN, NuMA, and dynein to the cell cortex to help orient the mitotic spindle. Mol. Cell. Biol. *30*, 3519–3530.

Xiao, Z., Wan, Q., Du, Q., and Zheng, Z. (2012). Galpha/LGN-mediated asymmetric spindle positioning does not lead to unequal cleavage of the mother cell in 3-D cultured MDCK cells. Biochem. Biophys. Res. Commun. *420*, 888–894.

Yang, S., Weng, H., Chen, L., Guo, X., Parra, M., Conboy, J., Debnath, G., Lambert, A.J., Peters, L.L., Baines, A.J., et al. (2011). Lack of protein 4.1G causes altered expression and localization of the cell adhesion molecule nectin-like 4 in testis and can cause male infertility. Mol. Cell. Biol. *31*, 2276–2286.

Ye, K., Compton, D.A., Lai, M.M., Walensky, L.D., and Snyder, S.H. (1999). Protein 4.1N binding to nuclear mitotic apparatus protein in PC12 cells mediates the antiproliferative actions of nerve growth factor. J. Neurosci. *19*, 10747–10756.